

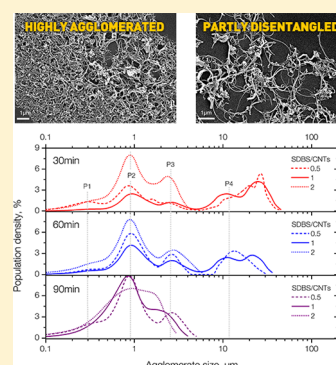
Optimization of Sonication Parameters for Homogeneous Surfactant-Assisted Dispersion of Multiwalled Carbon Nanotubes in Aqueous Solutions

Konstantinos G. Dassios,^{*,†} Panagiota Alafogianni,[†] Stelios K. Antiohos,[‡] Christos Leptokaridis,[‡] Nektaria-Marianthi Barkoula,[†] and Theodore E. Matikas[†]

[†]Department of Materials Science and Engineering, University of Ioannina, Ioannina GR-45110, Greece

[‡]Titan Cement Company S.A., Group R&D and Quality Department, Kamari Plant, P.O. Box 18, Elefsina 19200, Greece

ABSTRACT: The current study provides answers to two critical open questions concerning homogeneity of aqueous suspensions of carbon nanotubes by ultrasonic processing. The first is the dependence of tube dispersion quality on sonication duration and intensity, and the second is the identification of the appropriate conditions for retaining the highly desirable initial aspect ratio of the free-standing tubes in the dispersed state. A straightforward methodology based on nanotube agglomerate size analysis by liquid mode laser diffraction is suggested for quantifying the effects of sonication parameters on tube length and sample polydispersity. The technique, which is superior to currently suggested methods in that analysis of larger representative volumes is allowed and tube sedimentation effects are avoided, was tested across surfactant-assisted aqueous suspensions of multiwalled carbon nanotubes, while no apparent factors limit application to other types of suspensions. A ruling rationale for distinguishing between entangled states and individually suspended modes is presented, and the effects of surfactant concentration are discussed in the text. For the particular MWCNTs and experimental conditions investigated herein, an energy density rate of $7.7 \text{ J min}^{-1} \text{ mL}^{-1}$ applicable for a duration of 90 min was found optimum for achievement of suspension homogeneity without significant tube aspect ratio impairment.



1. INTRODUCTION

Carbon nanotubes (CNTs) are cylindrically shaped allotropes of carbon¹ known to exhibit a remarkable combination of structural,² mechanical,³ transport,⁴ optical, and electronic⁵ properties. While such assets have attracted intense scientific attention and have highlighted the one-dimensional nanoscale material as a prominent candidate in an ever-growing number of applications, it is also well-established that these qualifications cannot be fully exploited unless two characteristics, intrinsic to CNT nature, are overcome: their inherent hydrophobicity, which renders them immiscible in most common liquids, and their natural tendency to entangle and agglomerate under no external stimulus as a result of their high aspect ratios and large surface areas combined with strong van der Waals forces acting on their surface, with interaction energies of ca. 500 eV per micrometer of tube–tube contact.⁶

For many biomedical and engineering applications such as drug delivery systems⁷ and composite materials,⁸ CNT debundling and separation are absolute prerequisites in the production of homogeneous and stable suspensions during the processing phase. For example, in nanotube-reinforced materials, poor CNT dispersion within the continuous medium can result in inefficient material performance due to incomplete stress transfer between the phases, while CNT agglomerates can act as stress concentration sites promoting fatal crack initiation.⁹ In the ideal CNT-reinforced solid, tubes must be

dispersed and loaded individually for effective stress transfer and maximum toughening.

The most efficient resolution to the intrinsic hydrophobicity and self-entangling tendency of CNTs has proven to be modification of their outer walls, either covalently (chemically) or noncovalently (physically); the main principle behind both methods is the addition of solvent-friendly chemical moieties to the tubes' surfaces, which render them functional. Covalent CNT functionalization involves the nonreversible attachment, by means of chemical treatments/reactions, of functional appendages such as oxygen ($-\text{O}$), amino ($-\text{NH}_2$), and carboxyl ($-\text{COOH}$) groups on the tube sidewalls.¹⁰ While this type of functionalization offers tubes with high miscibility in a wide range of solvents, it is also known to hamper their physical and electronic properties by shortening tube length and perturbing their electronic cloud structure.¹¹ Noncovalent functionalization (NCF) involves the weak physical absorption of agent molecules on the tubes' surfaces by either hydrophobic interactions, Coulombic attractions, or π – π stacking interactions.¹² This type of functionalization is gaining much popularity lately over covalent bonding as it does not affect the chemical structure of the tube's graphene walls and can

Received: February 9, 2015

Revised: March 4, 2015

Published: March 5, 2015

improve the interfacial properties between the tubes and the dispersing medium.¹³ The main dispersive agents used in NCF are surfactants¹⁴ and polymers,¹⁵ while DNA and proteins have also been reported to interact noncovalently with CNTs in biosensing applications.¹⁶ In NCF, CNT dispersion is achieved mainly through ultrasonic processing of aqueous CNT suspensions containing low surfactant concentrations, up to a few wt %, ^{14b} while removal of larger CNT aggregates may require additional centrifugation.¹⁷ A detailed review unveiling the features and paths of sonochemistry is offered in ref 18. The absorption mechanism involves the strong attraction of the hydrophobic, nonpolar, tail segment of the amphiphilic surfactant molecule on the nanotube surface, while the hydrophilic, polar, headgroup interacts naturally with the surrounding solution.

To date, a number of methodologies have been suggested for evaluating the dispersion state of CNTs in aqueous solutions including atomic force microscopy (AFM),¹⁹ scanning and transmission electron microscopy (SEM and TEM),²⁰ UV–vis scanning,^{12,20a} fluorescence and Raman spectroscopy,²¹ small angle neutron scattering (SANS),²² and dynamic light scattering (DLS).²³ The limitations of spectroscopic and UV absorption techniques are related to the qualitative nature of information they can provide, such as relative percentages of tube agglomerate sizes in a given dispersion. Microscopy-based techniques require large statistical sample sizes and considerable manual postprocessing efforts for size measurements on wavy tubes and their agglomerates. Among the aforementioned methods, DLS is the most effective in measuring size distributions of nanotube agglomerates (assumed spherical) in suspension. A powerful variant of the technique, termed depolarized dynamic light scattering (DDLS), can provide realistic tube length estimates under the assumption of rod-like scatterers such as carbon nanotubes.^{23b,24}

The CNT dispersion mechanism under ultrasonic processing involves isolation of the tubes from their entangled/bundled state under the high shear forces exerted by the vibrating liquid. The forces act primarily at the bundle ends inducing the formation of intrabundle end-gaps that are propagated by further surfactant absorption in the newly separated tube surfaces.²⁵ According to one theory, a critical sonication time threshold exists where all bundles have successfully opened and, provided surfactant concentration is sufficient, all tubes have separated.²⁶ As the high shear forces that separate nanotubes can also fragment them,²⁷ sonication durations above this threshold can lead to decreases in tube aspect ratio and to downgrades of their mechanical and electrical/thermal transport performance. At the extreme end, surpassing the threshold by excessive time periods can have such detrimental effects as the complete destruction of the tubes and their conversion into amorphous carbon.^{19b,28} Another theory suggests that nanotube length deterioration commences immediately upon exposure to ultrasounds; in other words, unbundling cannot occur without nanotube shortening.^{19c,24b,29} In ref 19c, Hennrich et al. reported such behavior and found a power law dependence of tube length on sonication time, the power being -0.5 . Lucas et al. found a similar scaling dependence with the relevant power being -0.22 .^{24b} Pagani et al. rationalized the divergence by finding that both laws are correct and that each relates to a different of the two competing CNT fracture modes: buckling and stretching.^{29b} In a recent distinctive approach, Sesis et al. introduced cavitation energy, rather than input power, as the essential control parameter for tailoring

CNT dispersion.³⁰ Using a specialized experimental arrangement based on broadband monitoring of cavitation acoustic emission coupled with H₂O₂ production, two different cavitation types, stable and inertial, were identified, and several practical aspects relating to tip-based ultrasonication, surfactant degradation, and solution temperature were highlighted.

In practical terms and irrespective of whether nanotube shortening under sonication occurs after a certain time threshold or is continuous in time, knowledge of experimental parameters' values such as relevant time scales for unbundling CNTs without significant impairment of their aspect ratios is of paramount importance for future exploitation of CNT properties. This issue is still open today mainly due to the difficulty associated with characterizing CNT size in dispersion as well as dispersion homogeneity and stability.³¹ As a result, there is currently a vast selection of ultrasonication durations and energies, ranging from a few to hundreds of watts and from some minutes to days, reportedly capable of providing "homogeneous" dispersions of CNTs in surfactant-based aqueous solutions. Not only such a diversity highlights a current lack of convergence towards standardized procedures, even suggesting a high degree of arbitrariness in experimental practice but more frequently than not, even claimed homogeneity is only indirectly inferred and completely unsupported by dispersion quality data.

Clearly, exploitation of the 1-D material's properties is far from optimum, and a much deeper look is needed into the fundamentals of surfactant- and ultrasonics-assisted dispersion processes. Forward investigation and understanding of the mechanisms that enable CNTs to disperse homogeneously and interact individually in solutions, rather than inversely inferring such knowledge from indirect observations, is currently a necessity. Two key issues need to be resolved: (a) how CNT dispersion is affected by sonication duration and intensity and (b) whether CNT length and aspect ratio deterioration during ultrasonication can be avoided, and how. The current study aims to provide answers to these questions by presenting a straightforward methodology for quantifying the effects of sonication energy and duration on tube length and dispersion quality in surfactant-assisted aqueous dispersions of multiwalled carbon nanotubes (MWCNTs). The methodology relies on temporal CNT agglomerate size analysis by liquid mode laser diffractometry (LMLD),³² a technique popular for particle size analysis in the pharmaceutical industry, applied herein for the first time to carbon nanotubes. To efficiently relate ultrasonic processing intensity with dispersion quality and tube length characteristics, knowledge of the exact amount of vibrational energy transmitted to the nanotubes via ultrasonication is an imperative condition. To this end, the initial task of the study was calibration of this energy to basic experimental parameters. By identification of sonication-time-invariant peaks of disentangled CNTs in the LMLD size distribution curves of suspensions, optimum ultrasound energy densities and time scales for homogeneously dispersing the tubes without apparent impairment of their length are reported. The implications of the spherical particle assumption, the effect of spontaneous tube waviness in suspension, and the effects of surfactant concentration relatively to tube loading are also discussed.

2. EXPERIMENTAL SECTION

2.1. Materials. The multiwalled carbon nanotubes used in this study were synthesized via catalytic chemical vapor

deposition and are commercially available as “Long MWNT 2040” by Shenzhen Nanotech Port Co. Ltd., China. Figure 1

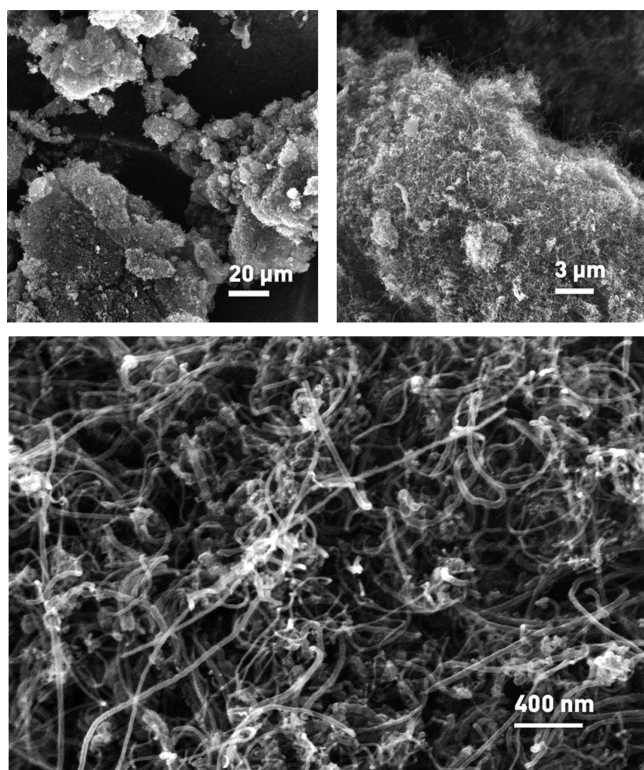


Figure 1. SEM images, at different magnifications, of bulk long multiwalled carbon nanotubes in the as-received, cotton-like entangled state.

shows scanning electron microscope (SEM) images of the cotton-ball-like form of as-received tubes at various length scales. Nominal tube diameter ranged from 20 to 40 nm (ca. 12–24 walls), while tube length ranged between 5 and 15 μm . Nominal sample purity was higher than 97% with less than 3% amorphous carbon and 0.2 wt % ash. Nominal special surface area of the tubes was 80–140 m^2/g , while their tapped density ranged from 0.15 to 0.28 g/cm^3 . Sodium dodecylbenzenesulfonate (SDBS, Sigma-Aldrich code 289957, Sigma-Aldrich Chemie GmbH, Munich, Germany), an anionic surfactant with a relatively high critical micelle concentration value of 1.5 mM, particularly popular for separation of nanotubes, was chosen as dispersion-assistive agent.³³

2.2. Methods. Ultrasonic processing for dispersion of tubes in suspension was performed with a Hielscher UP400S 24 kHz device (Hielscher Ultrasonics GmbH, Teltow, Germany), power capacity of 400 W, equipped with a $\varnothing 22$ mm cylindrical sonotrode. Output power was adjustable by means of wave amplitude regulation within 25–100%. The actual power transmitted to the suspension was measured with a Hielscher PowMet230 digital ultrasound energy meter.

Surfactant-assisted aqueous suspensions of MWCNTs were prepared in a fume hood environment according to the following methodology: A predetermined surfactant mass was initially added to 1000 mL of nondistilled water in 2000 mL capacity low form Pyrex glass beakers and an opalescent solution indicating complete SBDS dissolution was achieved after 60 s of magnetic stirring. The suspension volume of 1000 mL was selected as mean within the 100–2000 mL operational

range quoted by the manufacturer for the specific sonotrode. The sonotrode was subsequently fully immersed into the suspension (see section 3.1 for a discussion of the immersion depth effect), sonication was commenced, and 5 g of MWCNTs, quantity corresponding to a 0.5 wt % suspension concentration, was gradually introduced into the sonicated liquid. To avoid temperature increases in the bulk solution with ultrasonication duration, which would have a major influence on the dispersion efficiency,³⁰ the beaker was positioned in a bath with a continuous feed of fresh water. To investigate the effect of surfactant concentration on dispersion quality and identify the optimal surfactant/CNT ratio required to avoid surfactant stagnation or saturation, conditions which could respectively lead to only partial tube disentanglement or introduction of excess surfactant micelles in the bulk, suspensions with surfactant/CNT ratios of 1/2, 1/1, and 2/1 were prepared by varying the initial surfactant mass within 0.25, 0.5, and 1.0 g, respectively.

At tactical time intervals during ultrasonication, sample volumes of the suspensions were collected using a micropipette and transferred to the 400 mL water-filled liquid receptor vessel of a Cilas 1064 laser diffraction particle size analyzer (Cilas SA, Orleans, France). The operational principle of LMLD relies on the observation that the spatial distribution of light scattered from a liquid is proportional to the sizes of particles in suspension therein. Although LMLD shares the same assumption of spherical particles with DLS, it is superior to the latter in that the examined volume is not stationary during measurement but circulates in front of the analyzer laser beams. This not only prevents sedimentation and reagglomeration of CNTs during measurement, as the static conditions in DLS would enable, but also ensures examination of a larger, statistically more representative volume. The computer-controlled instrument is capable of analyzing particle sizes over the range from 4 nm to 500 μm in a single measurement by operating two sequenced laser sources positioned at 0° and 45°, to produce a diffraction pattern analyzed on a 64 channel silicon detector. Sample suspension volumes of ca. 8.0 mL provided in-vessel solutions of optic obscuration indices near 30% as required for accurate LMLD particle size analysis. Upon commencement of the measurement, the solution was mechanically stirred for 60 s and then circulated, for 60 s, through the internal piping system by aid of peristaltic micropumps. The acquisition stage of duration of 60 s commenced immediately after. After the end of each measurement, the size distribution curve of particles in suspension was represented as population density percentage versus CNT agglomerate size divided in 100 classes over the 0.04–500 μm range. The polydispersity index, PDI, of the distribution, a unitless measure of the heterogeneity of the sizes in suspension, was calculated from pair values of D_i , the agglomerate size value for class i , and $Q_3(x_i)$, the cumulative value representing the proportion of the sample with size equal to or less than x_i , through:

$$\text{PDI} = \frac{\sigma^2}{D_{\text{mean}}^2} \quad (1)$$

where σ is the sigma parameter of the log-normal law and D_{mean} is the mean agglomerate size value. These parameters are given by

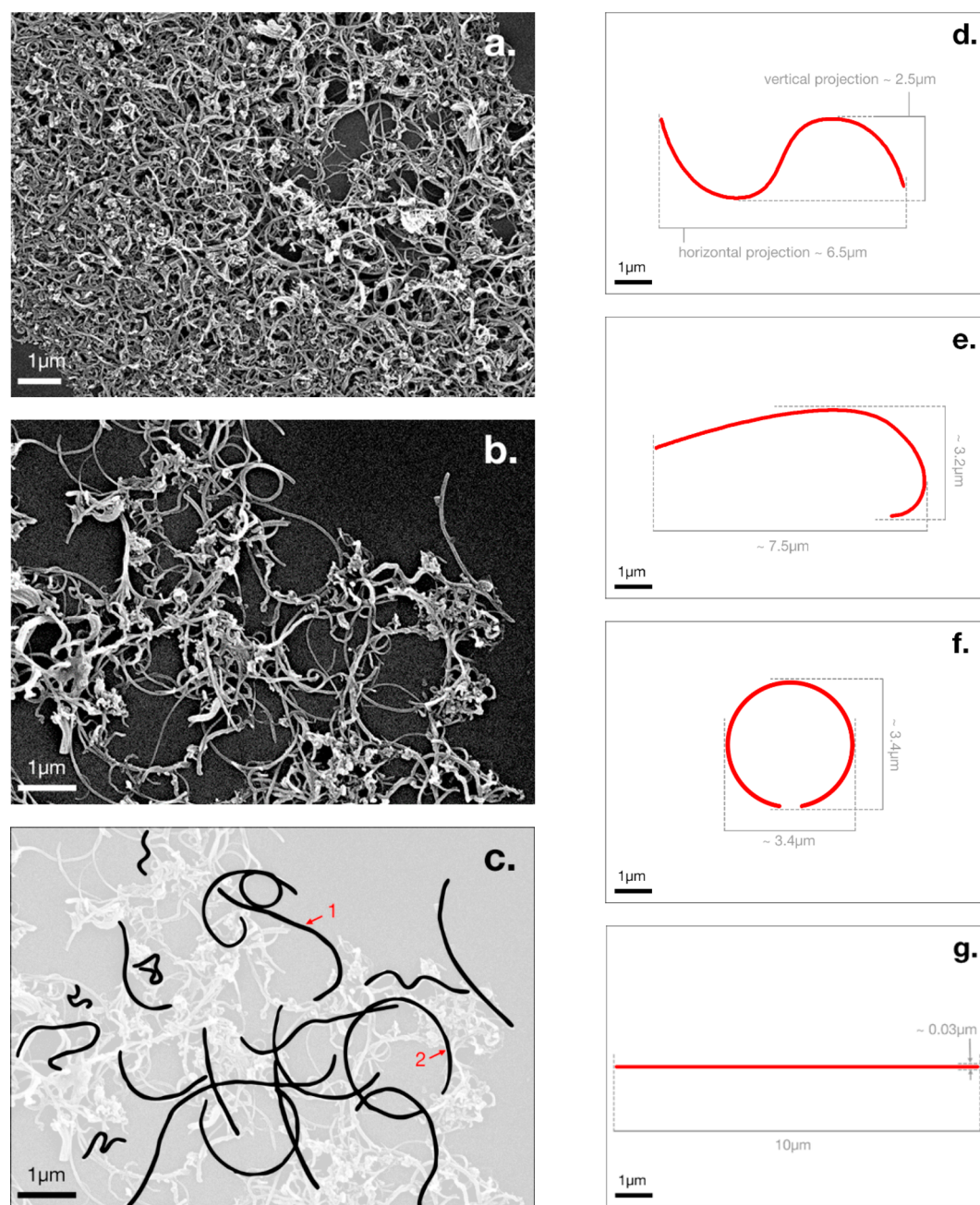


Figure 2. Typical tube shapes encountered in SDBS-assisted aqueous suspensions for perception of LMLD-measurable sizes. (a) Highly agglomerated tubes after 1 min of ultrasound processing and (b) disentangled tubes after 60 min of processing. (c) Isolation of typical modes encountered in (b). (d–g) Simulation of possible shapes of 10 μm -long CNTs and identification of their LMLD-measurable optical projections: (d) sigmoidal mode associated with minimum vertical projection, (e) “hook” mode associated with maximum horizontal projection, (f) “ring” mode with equal horizontal and vertical projections, and (g) perfectly straight tubes – condition not expected in an external-stimulus-free suspension.

$$\sigma = \sum_{i=1}^n D_i - D_{\text{mean}} \quad (2)$$

and

$$D_{\text{mean}} = \sum_{i=1}^n (P_i \cdot MD_i) \quad (3)$$

where n is the number of classes, in this case 100, P_i is the probability associated with class i , and MD_i is the mean agglomerate size value for class i . P_i and MD_i can be calculated from

$$P_i = Q_3(x_i) - Q_3(x_{i-1}) \quad (4)$$

and

$$MD_i = \frac{D_i + D_{i+1}}{2} \quad (5)$$

The PDI value of each distribution was used for evaluating dispersion quality; as a general rule, index values higher than 0.5 are considered associated with polydisperse/nonhomogeneously distributed samples.

2.3. Interpretation of LMLD Size Distribution Curves. LMLD reports particle size distributions by measuring the

angular variations in scattered light intensity as a laser beam passes through a flowing suspension of particulates in liquid. The size of particles, which are assumed spherical, is inversely proportional to the angle between the incident beam and scattered light, with large particles scattering light at small angles and vice versa. Using the Fraunhofer theory of light scattering, angular scattering intensity data are analyzed to calculate the size of the particles responsible for creating the captured scattering pattern. To interpret size, and changes therein, of nonspherical particles such as nanotubes from LMLD distribution curves, it is crucial to observe that the reported particle size value essentially corresponds to the equivalent sphere diameter that could reproduce the obtained data. While the shape of entangled CNT agglomerates may conditionally satisfy the spherical particle assumption, individually dispersed tubes will have higher aspect ratios, hence different laser diffraction patterns and different size distributions, depending on their instant orientation with respect to the laser beam. The situation gets more complicated upon consideration of the fact that the same scatterer can provide different diffraction patterns of the fact that in time, hence also different size distributions, due to the spontaneous motion of tubes in the surfactant-assisted suspension. The phenomenon is eventually masked by the vast population of CNTs in suspension and the correspondent randomness in orientations encountered by the incident beam, which leads to a realistic averaging of acquired sizes.

To evaluate length changes and distinguish between agglomerates and individual disentangled tubes, setting of ruling conditions is indispensable. As even in the -desirable-disentangled state, individual nanotubes are not expected to rest straight in an external-stimulus-free suspension but rather in a wavy arrangement, their horizontal and vertical optical projections, which will be interacting with and captured by the laser beam, will be only fractions of their nominal lengths. In fact, it is the degree of this waviness that defines the magnitude of discrepancy between the LMLD-reported size and real tube length. This effect is portrayed in Figure 2, which shows typical tube shapes encountered in suspension. The shapes were acquired by SEM imaging on microdroplets collected in situ during ultrasonic processing of the suspensions, placed on mica substrates, dried for 24 hr and subsequently gold-coated for enhanced electron conductivity. It is anticipated that the tubes partially reaggregate as the droplet volume is limited to two dimensions during spreading on the flat mica surface; this spreading however is not expected to interfere with their size or shape. Figure 2a and b shows successive time instances, at equivalent magnifications, of tubes in a SDBS-assisted suspension produced within the framework of the current study; the images show the effect of sonication duration on tube disentanglement. For ease of morphology perception, profound tube shapes encountered in Figure 2b were isolated by aid of image analysis software, as shown in Figure 2c, and their projections were found consistently smaller, within 30–70%, than their straight lengths, due to their inherent waviness ranging from slightly bent, as for example in nanotube denoted “1” in Figure 2c, to almost circular (nanotube “2” in same figure).

A classification of CNT shapes into major modes and a correlation of their projections to actual tube length become particularly significant. Figures 2d–g present simulations of such shape possibilities for a 10 μm long nanotube (mean of the 5–15 μm range of the tubes of this study). The values of

both horizontal and vertical optical projections of the shapes, which constitute the LMLD-measurable parameter, are reported in each figure. Figure 2g represents the unrealistic, upper-bound scenario of perfectly straight nanotubes and is included only for comparison purposes. It is observed that, for 10 μm long tubes, the minimum optical projection is 2.5 μm for the sigmoidal shape of Figure 2d, while the maximum projection is 7.5 μm and corresponds to the hook-like shape of Figure 2e. This 25–75% difference between LMLD-measured length and actual tube length was established for plane conditions; considering that waviness of the freely suspended tubes in the aqueous volume would extend also in the third dimension, it is anticipated that the LMLD-sensed optical projections would be further reduced, possibly by the same additional percentage. Taking this into account, a rough calculation of the LMLD size range for individually suspended tubes is possible by applying the second power of the minimum (25%) and maximum (75%) reduction on the lower and upper ends of the 5–15 μm length range, respectively. This gives the range of 0.3–8.4 μm , which essentially corresponds to the LMLD-measurable size range for unshortened 10 μm -long nanotubes in an ideal homogeneous dispersion. Because of the simplicity of the aforementioned approach and the limited shape modes simulated in Figure 2d–f, this range can be utilized as approximation only. It is, nonetheless, safe to apply the minimum reduction (25%) to the maximum of the 5–15 μm range, to establish a conservative upper threshold for separated tubes as 11.2 μm . It can then be ruled that, for the tubes of this study, population density peaks above ca. 11.2 μm may correspond to entangled states only. Peaks appearing below this threshold may correspond to either unshortened individually dispersed tubes, which would constitute an ideal homogeneous dispersion, or agglomerates of much shortened (by initial state or by ultrasound) tubes.

3. RESULTS AND DISCUSSION

3.1. Energy Transmitted to the Tubes. Understanding how ultrasonic processing intensity affects dispersion quality and tube length requires knowledge of the exact amount of vibrational energy transmitted to the nanotubes. Hence, the primary task of the study was to accurately measure the power sensed by CNTs in suspension by varying not only basic experimental parameters such as wave amplitude but also subjective, user-dependent parameters such as sonotrode immersion depth. Figure 3 presents isoamplitude calibration contours of the rate of change of ultrasound vibrational energy, transmitted to a 1 wt % suspension of MWCNTs in 1000 mL of water within a standard high-form 2000 mL beaker, SDBS/CNT ratio of 1, for different wave amplitude selections and sonotrode immersion depths. As expected, power (energy rate) is seen to increase with wave amplitude for all immersion depths; this variation appears to be close to linear: for example, at 30 mm immersion, power doubles from 6000 to 12 000 J/min as wave amplitude increases from 50% to 100%. Interestingly, sonotrode immersion itself appears to play a significant role to the rate of energy transmitted to the nanotubes. For example, the amount of power transmitted to the tubes in suspension at 25% wave amplitude increases from 4096 to 5410 J/min, a change of ca. 32%, as tip immersion increases from 5 to 45 mm. At 100% wave amplitude, the increase in power for the same immersion range is much higher, 46%. This finding indicates that, although power may vary linearly with amplitude for the same immersion depth, power

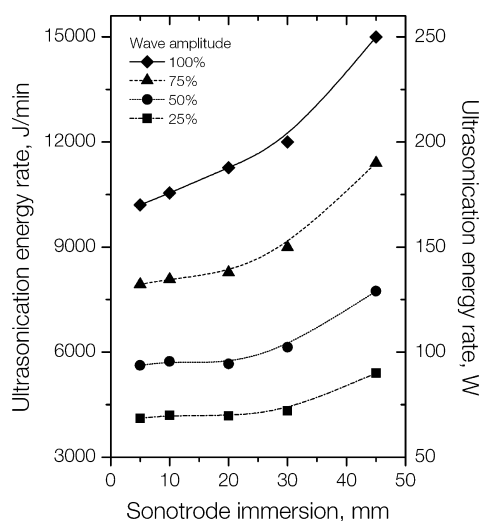


Figure 3. Isoamplitude power calibration contours as a function of sonotrode immersion depth, for different wave amplitude selections.

variation with immersion depth gets steeper as amplitude increases. This effect is demonstrated as a “hand fan” behavior in the isoamplitude contours of Figure 3. The established dependence of power transmitted to the nanotubes on tip immersion depth which, to the authors' knowledge, has not been previously reported in the literature, is of particular importance for experimental practice. It signifies that careful selection of immersion depth and wave amplitude is crucial for providing the tubes in suspension with the rate of energy required for efficient separation without the adverse side-effects of insufficient or excessive sonication. In a practical example, the data of Figure 3 indicate that the amount of power delivered to the tubes by a fully immersed sonotrode operating at 75% of the wave amplitude is equal to a half-immersed one operating at 100% amplitude. Thus, regulating the amplitude is as important as selecting the correct immersion depth. Lack of such knowledge may not be unrelated to the current diversity in reported sonication powers and durations for producing homogeneous CNT suspensions. The situation gets much more complex when the different sonotrode geometries, dimensions and ultrasound frequencies of the various ultrasonics equipment available for research come into play. The isoamplitude power contours of Figure 3 are useful as guides for the selection of sonotrode immersion depth and wave amplitude combinations required to transmit a desired rate of ultrasonication energy to CNT in suspension, or for evaluating energy requirements to moderate or intensify sonication effects for improving dispersion quality and avoiding CNT aspect ratio impairment.

3.2. Optimization of Ultrasonication Parameters. To avoid the side effects of oversonication while capturing the incremental role of sonication parameters, the work rationale followed in the present study consisted of a bottom-up approach starting from mild sonication intensities and durations. Identification of optimal sonication conditions for achievement of homogeneous suspensions of nanotubes with minimum length impairment was performed in terms of quantifying the shifts of population density peaks in CNT agglomerate size distributions. Figure 4 presents CNT agglomerate size distributions for MWCNT suspensions exposed for durations of 1, 5, and 30 min to low sonication energies rates of 5400 J/min, achieved by means of wave

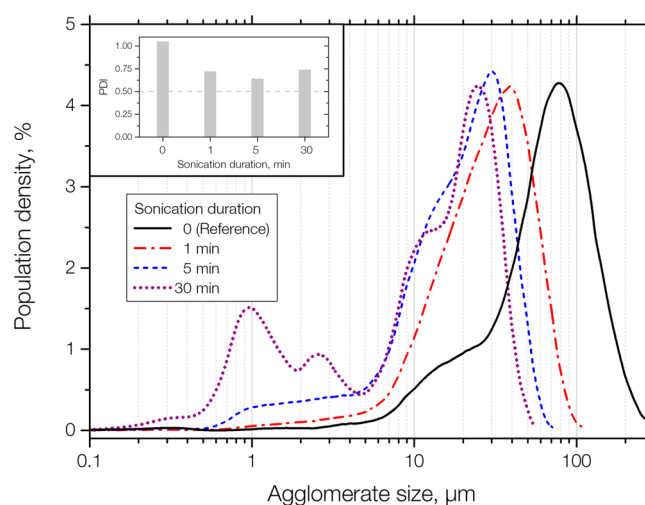


Figure 4. CNT agglomerate size distribution curves and associated PDI indices for different sonication durations at a mild ultrasonication energy rate of 5400 J/min.

amplitude regulation to 25% of the instrument capacity. For reference purposes, the size distribution curve of an unsonicated sample is also included in the graph, plotted as a solid line. The cumulative vibrational energy transmitted to the suspensions for 1, 5, and 30 min can be calculated as 5.4, 27, and 162 kJ, respectively. On the basis of the argumentation presented in section 2.3, as all peaks of sonicated samples in Figure 4 appear well above 20 μm , neither energy is considered sufficient for deagglomerating the tubes. The profound peak appearing initially at 80 μm (unsonicated sample) shifted to 40 μm after only 1 min of ultrasonic processing (dashed-dotted line), still associated with heavily entangled conditions. The peak shifts to 30 μm after 5 min of processing (dashed line), evidently inflated toward the 11.2 μm threshold. It is only after transmission of 162 kJ of energy to the tubes (30 min of sonication, dotted line) that the peak eventually splits with the appearance of contributions at 0.3, 0.9, 2.5, and 11.5 μm , possibly corresponding to disentangled states, while the majority of the population is still entangled around the peak at 25 μm . The PDI values of the distributions (subset graph of Figure 4) drop from the extreme reference value of ca. 1.0 to the vicinity of 0.7, signifying low homogeneity in all suspensions.

The same MWCNT suspensions previously ultrasonicated with 5.4, 27, and 162 kJ of energy were left to rest for a time period of 3 days to allow suspended nanotubes to reach thermodynamic equilibrium. Suspensions were then analyzed again in terms of agglomerate sizes (without further sonication), and the resulting distributions are plotted in Figure 5 (solid lines) alongside the original behaviors after 1, 5, and 30 min of sonication (dashed lines). While all 3-day distributions appeared highly heterogeneous with well-defined peaks at separated positions and the corresponding PDI values were even higher than before, the locations of several peaks below 12 μm were observed to remain unaffected by initial sonication duration. The peaks at 0.3 (P1), 0.9 (P2), 2.5 (P3), and 11.5 μm (P4) previously encountered in 30 min-sonicated samples now appear also in the 1 and 5 min equilibrated samples. Above 12 μm , peaks appear at inconstant locations among different samples with the prominent peak at 40 μm of the equilibrated sample 1 min-sonicated sample having shifted

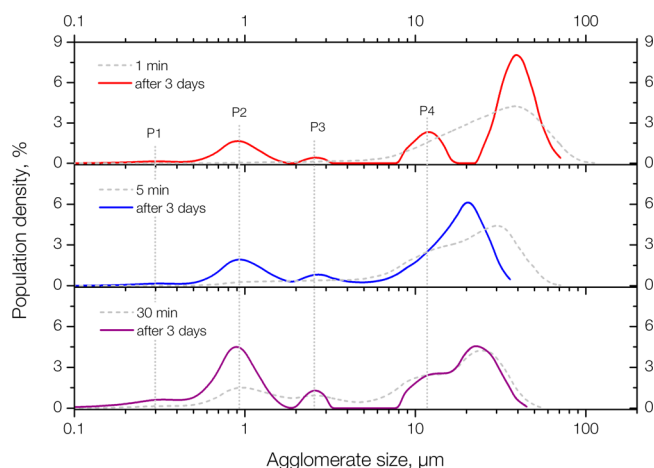


Figure 5. CNT agglomerate size distribution curves, following a 3-day rest for achievement of thermodynamic equilibrium, of suspensions previously ultrasonicated at a mild energy rate of 5400 J/min.

to ca. 25 μm in the equilibrated 30 min-sonicated samples. It is interesting to note that the differentiation in peak position constancy occurs above a size class, 11.5 μm , which compares favorably with the entanglement threshold estimate of 11.2 μm calculated for wavy tubes of total lengths of 5–15 μm (see Section 2.3). Hence, allowed nanotube size modes (peaks 1–4) are specific and repetitive below the entanglement threshold; that is, under the ultrasonication configuration of the present study, tubes can only separate to fixed agglomerate sizes. The inconstancy in peak position above the threshold is a finding that independently validates the claim that these peaks correspond to entangled states only. For these states, sonication energies of 5.4, 27, and 162 kJ appeared insufficient for complete disentanglement.

The above results indicate that tube suspension homogeneity requires input of more drastic vibrational energies levels. An increase in vibration energy rate input rather than duration was deemed appropriate. Figure 6 represents CNT agglomerate size distributions for MWCNT suspensions exposed for durations of 1, 5, and 30 min to sonication energies rates of 7700 J/min, by means of wave amplitude regulation to 50% of the

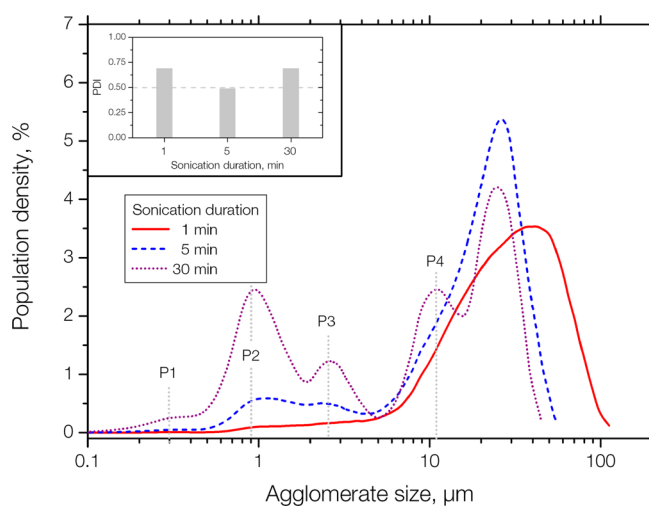


Figure 6. CNT agglomerate size distribution curves and associated PDI indices for different sonication durations at an ultrasonication energy rate of 7700 J/min.

instrument capacity. The cumulative vibrational energy transmitted to the suspensions for each of the above durations can be calculated as 7.7, 38.5, and 231 kJ, respectively. In this case, the vibrational energy level appeared sufficient of revealing modes P1, P2, and P3, at 0.3, 0.9, and 2.5 μm , respectively, at durations as low as 5 min (dashed line), while 1 min of exposure appeared again too low for the same purpose. 231 kJ of vibrational energy (30 min of sonication) resulted in well-defined P1, P2, P3, and P4 modes of intensities now comparable to the entangled states above the 11.2 μm threshold. PDI values consistently above 0.5 also indicate polydisperse samples.

Evidently, homogeneity cannot be achieved unless the energy input is increased to the situation that all entangled states shift to the allowable modes below P4. To this end, sonication duration was increased to 60, 90, and 120 min, which enabled transmission of 462, 693 and 924 kJ, respectively, to the nanotubes in suspension. Figure 7 represents CNT agglomerate

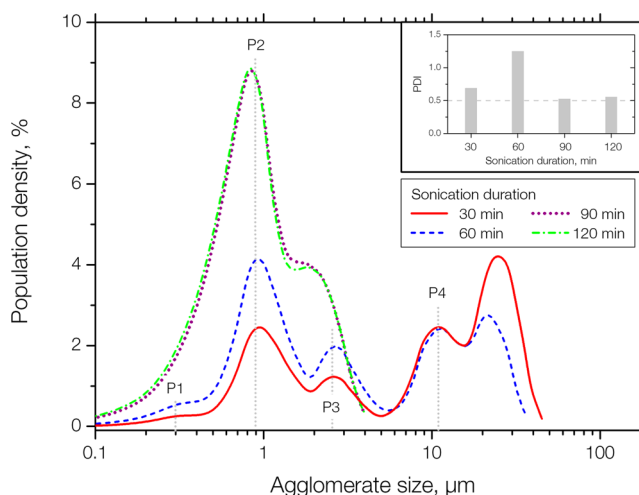


Figure 7. CNT agglomerate size distribution curves and associated PDI indices for prolonged sonication durations at an ultrasonication energy rate of 7700 J/min.

size distributions for suspensions exposed to such vibrational energy levels. It is observed that after 60 min of ultrasonication at the same energy rate as before (7700 J/min, dashed line), the outermost peak at 30 μm reduces in favor of P1, P2, and P3 modes, which now exhibit higher intensity than peaks of entangled states. It is interesting that transmission of another 231 kJ of energy (total of 90 min of ultrasonication, dotted line) results in the vanishing of the P4 mode at ca. 11 μm and the merging of P1, P2, and P3 in a convoluted mode around P2, compatibly with desirable monodispersity conditions. The maximum size in the new peak is 4 μm . Most importantly, transmission of another 231 kJ of ultrasound energy (total of 120 min of ultrasonication, dotted line) has absolutely no effect on peak location and intensity, a finding that signifies that nanotube disentanglement is already complete at 90 min. The PDI values drop from 0.7 and 1.25 for 30 and 60 min of ultrasonication, respectively, to an acceptable 0.5 for a sonication duration of 90 min, the index value that does not change considerably with further energy transmission to the suspension.

It is hence partially concluded that an ultrasound vibrational energy input rate of 7700 J/min over a time period of 90 min is sufficient for homogeneously distributing 0.5 g of carbon

nanotubes in a 1000 mL aqueous suspension. As experimental protocols require robust recipes, unification of the above information in a single, handier, measure appears as a challenging task. One such measure could, for example, be “energy density per gram of suspended CNTs”, devised as energy rate multiplied by duration, divided by suspension volume and total tube mass. During the study, it was found that the energy transmitted to the suspension remains practically constant for nanotube concentrations up to a few percent weight, which is sufficient for most biomedical, reinforcing, sensing, and electrical/thermal transport applications. Thus, for low CNT loadings, a simple quotation of the energy density would appear sufficient. On the basis of the findings of the present study, that property is calculated as 693 J/mL. Unfortunately, one cannot unconditionally equalize the time and energy rate dependencies by unifying them into one single term. This is because it is still uncertain whether their synergy is linearly coupled with exactly inverse dependencies, that is, whether higher energy rates applicable for short durations can achieve the same dispersion characteristics as lower energy rates applicable for longer durations. Nonetheless, for the purposes of this study, application of an energy density rate of 7.7 J min⁻¹ mL⁻¹ for a duration of 90 min can be quoted as satisfactory for achieving homogeneity in the aqueous suspensions of investigated MWCNTs.

3.3. Effect of Surfactant Concentration. Given the surfactant’s predominant role in nanotube separation, hence also suspension homogeneity, an investigation of the effect of perturbing its concentration, on dispersion quality appears relevant. Figure 8 depicts agglomerate size distribution curves

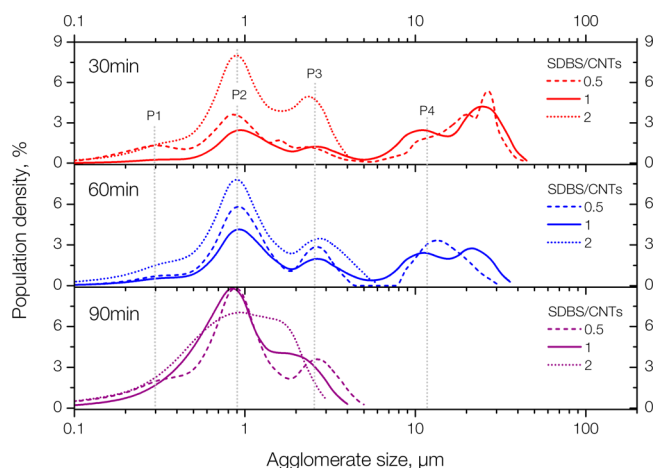


Figure 8. Effect of surfactant to CNT loading ratio on dispersion quality for 30, 60, and 90 min of sonication duration at energy rate of 7700 J/min.

of suspensions exposed to an ultrasonication energy rate of 7700 J/min for 30, 60, and 90 min with varying SDBS/CNT loading ratios of 0.5, 1, and 2. For ease of comparison, the previously established behaviors corresponding to SDBS/CNT ratios of 1 are represented with solid lines, whereas ratios of 0.5 and 2 are plotted dashed and dotted, respectively. It is observed that for all sonication durations, decreasing the surfactant concentration to one-half the tube loading does not have a significant effect on dispersion quality, with peaks of comparable intensity appearing above the entanglement threshold in common for SDBS/CNT loading ratios of 0.5 and 1. On the other hand, increasing the surfactant

concentration 2-fold the tube concentration, has impressive results on dispersion quality even for sonication durations as low as 30 min, where complete absence of entangled states is observed. In fact, the condition portrayed for a sonication duration of 30 min and a SDBS/CNT ratio of 2 is equivalent to the one previously established as optimal for a duration of 90 min and a corresponding ratio of 1. This observation signifies that surfactant excess can assist in establishment of homogeneity conditions with smaller energy input requirements. Such excess however is not without side-effects in terms of application potential¹² and should not be preferred over the combination of moderate SDBS/CNT ratios and longer ultrasonication durations. It is also interesting to note that prolonged sonication helps the establishment of homogeneity and smoothing out most of the differences, regardless of surfactant concentration. For example, after 90 min of sonication at 7700 J/min, SDBS/CNT ratios as low as 0.5 are sufficient for complete disentanglement of the tubes, as shown by the dashed line of the 90 min graph. Most interestingly, the behavior portrayed in Figure 8 indicates that the location of allowable size modes P1, P2, and P3 appears invariant to surfactant concentration. This means that size modes below the threshold do not depend on the amount of the dispersion-assistive agent. Such a condition can only be satisfied by individual tubes and not by agglomerates of shortened (by initial state of by ultrasonication) tubes. If modes P1, P2, and P3 corresponded to entanglements of shorter tubes, they would break down to their smaller constituents with increasing SDBS loading. In fact, as suggested by the changes in peak intensity with surfactant ratio, increasing the amount of surfactant appears to only assist the disentanglement of more of the larger agglomerates to the already allowable modes. This finding is important in view of the necessity in understanding whether CNT length, hence also aspect ratio, deteriorates during ultrasonication. The forward-approach methodology presented in this study, starting from conservative sonication conditions, appears capable of providing homogeneous MWCNT suspensions without length impairment, because the same individual nanotube size modes present in a mildly sonicated sample (sonication for 1 min at 5400 J/min) are also present in the optimally homogeneous suspension (sonication for 90 min at 7700 J/min).

It must be recalled that due to the naturally expected waviness of nanotubes in an aqueous environment, the sizes captured by LMLD are only a fraction of actual CNT length. Using the minimum and maximum length reduction factors established in section 3.2 as 0.25² and 0.75², respectively, the length of nanotubes appearing in modes P1–P4, from 0.3 to 11.5 μm, respectively, can be approximated as 4.8–20.4 μm. While the lower end of the established range compares favorably with the minimum length of 5 μm quoted by the manufacturer, the upper end overestimates the corresponding nominal value of 15 μm. This finding may not be unrelated to the fact that mode P4 is not encountered in the homogeneously dispersed sample after 90 min of ultrasonic processing.

3.4. Power Law Dependence. The finding of the current study that individually dispersed CNT modes P1, P2, and P3 are consistently present in the distribution curves of all ultrasonication durations appears supportive of the theory that nanotube disentanglement can occur without significant degradation in original nanotube length, hence also aspect ratio. It must be noted that opposing theories, claiming that nanotube shortening commences immediately upon exposure to ultra-

sonication, with relevant power law exponents of -0.22^{24b} and -0.5^{19c} are based on mean agglomerate sizes derived from single-peak distributions; these peaks were trivially accommodated by Gaussian/Lorentzian curves. Such monodispersity conditions are radically simpler than the multiplex behavior captured for the CNT suspensions of the present study, especially in suspensions prior to achievement of homogeneity. Equation 3 allows calculation of a mean size even for polydispersity conditions, and although such a value would not be equivalent to the mean of a monodisperse sample, an attempt is made to compare the current findings to literature results. The variation of the mean size of the distributions as a function of ultrasonication duration, t , for a SDBS/CNT ratio of 1 and an energy density rate of $7.7 \text{ J min}^{-1} \text{ mL}^{-1}$ is presented in Figure 9; for ease of comparison with literature, the $t^{-0.22}$ and

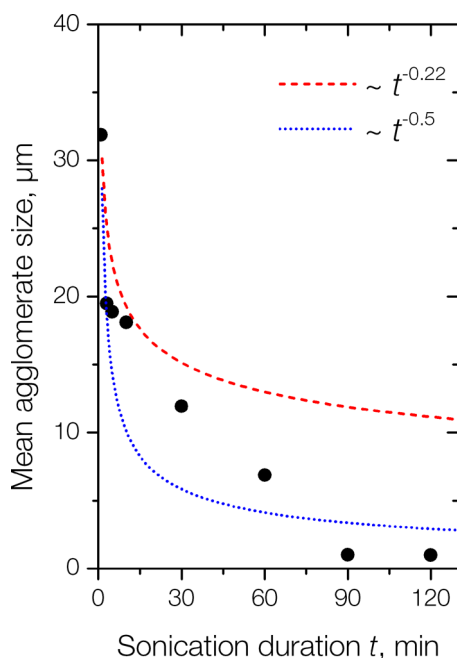


Figure 9. Mean agglomerate size as a function of sonication duration, and competing power law behaviors, at an energy density rate of $7.7 \text{ J min}^{-1} \text{ mL}^{-1}$ and surfactant-to-CNT ratio of 1.

$t^{-0.5}$ power law behaviors are included in the graph. It is observed that, although the majority of the data remains well within the two laws' region, the shape of the data does not match any of the simulated behaviors. This does not necessarily imply that the two competing CNT fracture mechanisms under ultrasonication, buckling and stretching,^{29b} are not present in the suspensions under investigation but rather that CNT disentanglement into the individually dispersed modes P1, P2, and P3 occurs prior to CNT scission by any of the mechanisms.

4. CONCLUSIONS

The current study reports a viable methodology for achievement of surfactant-assisted homogeneous dispersions of MWCNTs in aqueous solutions by optimization of sonication parameters such as duration, energy, and surfactant loading ratio. To avoid impairment of tube length, a forward approach was followed starting from mild sonication intensities and durations and scaling up until homogeneity was established. Key findings include:

- Calibration curves of the rate of vibrational energy transmitted to MWCNT suspensions revealed a strong dependence of the energy not only on wave amplitude but also on sonotrode immersion depth.
- The effect of spontaneous nanotube waviness on size acquired by scattering/diffraction techniques operating under the spherical particle assumption and its correlation to actual tube length was demonstrated by simulation of possible shapes of tubes in suspension.
- Temporal and spatial analysis of CNT agglomerate size distributions was performed via the liquid mode laser diffraction technique, herein applied for the first time to nanotube suspensions. Superior to currently suggested similar methods, LMLD allows analysis of larger, statistically more representative, volumes, while it ensures avoidance of tube sedimentation effects.
- Shifts in population density peaks acquired via the LMLD method enabled identification of allowable nanotube size modes at 0.3, 0.9, and $2.5 \mu\text{m}$.
- The locations of these modes remained invariant to sonication intensity and surfactant concentration and were hence attributed to individually suspended tubes.
- The entanglement threshold above which only entangled states exist in the suspension was established as $11.5 \mu\text{m}$ for the $5\text{--}15 \mu\text{m}$ long tubes.
- An energy density rate of $7.7 \text{ J min}^{-1} \text{ mL}^{-1}$ applicable for a duration of 90 min was found optimum for achievement of homogeneous suspensions without CNT aspect ratio impairment for the MWCNTs and experimental conditions specific to the current study.
- The agglomerate size versus sonication duration data were not successfully approximated by power law behaviors currently suggested in the literature.

The suggested methodology is material-invariant and can hence be applied to other types of nanoscale carbon suspensions such as single-walled carbon nanotubes and graphene, or to noncarbonaceous matter.

AUTHOR INFORMATION

Corresponding Author

*Tel.: +30-26510-09010. Fax: +30-26510-09066. E-mail: kdassios@cc.uoi.gr.

Notes

The authors declare no competing financial interest.

ACKNOWLEDGMENTS

This research project has been cofinanced by the European Union (European Regional Development Fund – ERDF) and Greek national funds (General Secretariat for Research and Technology) through the Operational Program “Competitiveness and Entrepreneurship and Regions in Transition” of the National Strategic Reference Framework (NSRF 2007-2013), under the program “Cooperation 2011, Partnerships of Production and Research Institutions in Focused Research and Technology Sectors”.

REFERENCES

- (1) Iijima, S. Helical Microtubules of Graphitic Carbon. *Nature* **1991**, *354*, 56–58.
- (2) Wang, X. S.; Li, Q. Q.; Xie, J.; Jin, Z.; Wang, J. Y.; Li, Y.; Jiang, K. L.; Fan, S. S. Fabrication of Ultralong and Electrically Uniform Single-Walled Carbon Nanotubes on Clean Substrates. *Nano Lett.* **2009**, *9*, 3137–3141.

- (3) (a) Treacy, M. M. J.; Ebbesen, T. W.; Gibson, J. M. Exceptionally high Young's modulus observed for individual carbon nanotubes. *Nature* **1996**, *381*, 678–680. (b) Yu, M. F.; Lourie, O.; Dyer, M. J.; Moloni, K.; Kelly, T. F.; Ruoff, R. S. Strength and breaking mechanism of multiwalled carbon nanotubes under tensile load. *Science* **2000**, *287*, 637–640.
- (4) (a) Balandin, A. A. Thermal properties of graphene and nanostructured carbon materials. *Nat. Mater.* **2011**, *10*, 569–581. (b) Berber, S.; Kwon, Y. K.; Tomanek, D. Unusually high thermal conductivity of carbon nanotubes. *Phys. Rev. Lett.* **2000**, *84*, 4613–4616. (c) Baughman, R. H.; Zakhidov, A. A.; de Heer, W. A. Carbon nanotubes - the route toward applications. *Science* **2002**, *297*, 787–792.
- (5) (a) Avouris, P.; Chen, Z. H.; Perebeinos, V. Carbon-based electronics. *Nat. Nanotechnol.* **2007**, *2*, 605–615. (b) Avouris, P.; Freitag, M.; Perebeinos, V. Carbon-nanotube photonics and optoelectronics. *Nat. Photonics* **2008**, *2*, 341–350.
- (6) (a) Harris, P. J. F. Carbon nanotube composites. *Int. Mater. Rev.* **2004**, *49*, 31–43. (b) Girifalco, L. A.; Hodak, M.; Lee, R. S. Carbon nanotubes, buckyballs, ropes, and a universal graphitic potential. *Phys. Rev. B* **2000**, *62*, 13104–13110.
- (7) Zhang, W. X.; Zhang, Z. Z.; Zhang, Y. G. The application of carbon nanotubes in target drug delivery systems for cancer therapies. *Nanoscale Res. Lett.* **2011**, *6*.
- (8) Spitalsky, Z.; Tasis, D.; Papagelis, K.; Galiotis, C. Carbon nanotube-polymer composites: Chemistry, processing, mechanical and electrical properties. *Prog. Polym. Sci.* **2010**, *35*, 357–401.
- (9) Xie, X. L.; Mai, Y. W.; Zhou, X. P. Dispersion and alignment of carbon nanotubes in polymer matrix: A review. *Mater. Sci. Eng., R* **2005**, *49*, 89–112.
- (10) (a) Datsyuk, V.; Kalyva, M.; Papagelis, K.; Parthenios, J.; Tasis, D.; Siokou, A.; Kallitsis, I.; Galiotis, C. Chemical oxidation of multiwalled carbon nanotubes. *Carbon* **2008**, *46*, 833–840. (b) Dyke, C. A.; Tour, J. M. Covalent functionalization of single-walled carbon nanotubes for materials applications. *J. Phys. Chem. A* **2004**, *108*, 11151–11159.
- (11) (a) Collins, P. G.; Bradley, K.; Ishigami, M.; Zettl, A. Extreme oxygen sensitivity of electronic properties of carbon nanotubes. *Science* **2000**, *287*, 1801–1804. (b) Kim, B.; Park, H.; Sigmund, W. M. Electrostatic interactions between shortened multiwall carbon nanotubes and polyelectrolytes. *Langmuir* **2003**, *19*, 2525–2527.
- (12) Blanch, A. J.; Lenehan, C. E.; Quinton, J. S. Optimizing Surfactant Concentrations for Dispersion of Single-Walled Carbon Nanotubes in Aqueous Solution. *J. Phys. Chem. B* **2010**, *114*, 9805–9811.
- (13) Kim, K. T.; Jo, W. H. Noncovalent Functionalization of Multiwalled Carbon Nanotubes Using Graft Copolymer with Naphthalene and Its Application as a Reinforcing Filler for Poly(styrene-co-acrylonitrile). *J. Polym. Sci., Part A: Polym. Chem.* **2010**, *48*, 4184–4191.
- (14) (a) Rastogi, R.; Kaushal, R.; Tripathi, S. K.; Sharma, A. L.; Kaur, I.; Bharadwaj, L. M. Comparative study of carbon nanotube dispersion using surfactants. *J. Colloid Interface Sci.* **2008**, *328*, 421–428. (b) Vaisman, L.; Wagner, H. D.; Marom, G. The role of surfactants in dispersion of carbon nanotubes. *Adv. Colloid Interface Sci.* **2006**, *128*, 37–46.
- (15) (a) Lou, X. D.; Daussin, R.; Cuenot, S.; Duwez, A. S.; Pagnouille, C.; Detrembleur, C.; Bailly, C.; Jerome, R. Synthesis of pyrene-containing polymers and noncovalent sidewall functionalization of multiwalled carbon nanotubes. *Chem. Mater.* **2004**, *16*, 4005–4011. (b) Carrillo, A.; Swartz, J. A.; Gamba, J. M.; Kane, R. S.; Chakrapani, N.; Wei, B. Q.; Ajayan, P. M. Noncovalent functionalization of graphite and carbon nanotubes with polymer multilayers and gold nanoparticles. *Nano Lett.* **2003**, *3*, 1437–1440.
- (16) Zheng, M.; Jagota, A.; Semke, E. D.; Diner, B. A.; Mclean, R. S.; Lustig, S. R.; Richardson, R. E.; Tassi, N. G. DNA-assisted dispersion and separation of carbon nanotubes. *Nat. Mater.* **2003**, *2*, 338–342.
- (17) O'Connell, M. J.; Bachilo, S. M.; Huffman, C. B.; Moore, V. C.; Strano, M. S.; Haroz, E. H.; Rialon, K. L.; Boul, P. J.; Noon, W. H.; Kittrell, C.; Ma, J. P.; Hauge, R. H.; Weisman, R. B.; Smalley, R. E. Band gap fluorescence from individual single-walled carbon nanotubes. *Science* **2002**, *297*, 593–596.
- (18) Cintas, P. T.; Caporaso, M.; Tabasso, S.; Cravotto, G. Enabling technologies built on a sonochemical platform: Challenges and opportunities. *Ultrason. Sonochem.* **2014**, <http://dx.doi.org/10.1016/j.ultrsonch.2014.12.004>, in press.
- (19) (a) Chen, Q.; Saltiel, C.; Manickavasagam, S.; Schadler, L. S.; Siegel, R. W.; Yang, H. C. Aggregation behavior of single-walled carbon nanotubes in dilute aqueous suspension. *J. Colloid Interface Sci.* **2004**, *280*, 91–97. (b) Islam, M. F.; Rojas, E.; Bergey, D. M.; Johnson, A. T.; Yodh, A. G. High weight fraction surfactant solubilization of single-wall carbon nanotubes in water. *Nano Lett.* **2003**, *3*, 269–273. (c) Hennrich, F.; Krupke, R.; Arnold, K.; Stutz, J. A. R.; Lebedkin, S.; Koch, T.; Schimmel, T.; Kappes, M. M. The mechanism of cavitation-induced scission of single-walled carbon nanotubes. *J. Phys. Chem. B* **2007**, *111*, 1932–1937.
- (20) (a) Yu, J. R.; Grossiord, N.; Koning, C. E.; Loos, J. Controlling the dispersion of multi-wall carbon nanotubes in aqueous surfactant solution. *Carbon* **2007**, *45*, 618–623. (b) Kerr, C. J.; Huang, Y. Y.; Marshall, J. E.; Terentjev, E. M. Effect of filament aspect ratio on the dielectric response of multiwalled carbon nanotube composites. *J. Appl. Phys.* **2011**, *109*.
- (21) (a) Moore, V. C.; Strano, M. S.; Haroz, E. H.; Hauge, R. H.; Smalley, R. E.; Schmidt, J.; Talmon, Y. Individually suspended single-walled carbon nanotubes in various surfactants. *Nano Lett.* **2003**, *3*, 1379–1382. (b) Shen, K.; Curran, S.; Xu, H. F.; Rogelj, S.; Jiang, Y. B.; Dewald, J.; Pietrass, T. Single-walled carbon nanotube purification, pelletization, and surfactant-assisted dispersion: A combined TEM and resonant micro-Raman spectroscopy study. *J. Phys. Chem. B* **2005**, *109*, 4455–4463. (c) Heller, D. A.; Barone, P. W.; Swanson, J. P.; Mayrhofer, R. M.; Strano, M. S. Using Raman spectroscopy to elucidate the aggregation state of single-walled carbon nanotubes. *J. Phys. Chem. B* **2004**, *108*, 6905–6909. (d) Kumatani, A.; Warburton, P. A. Characterization of the disaggregation state of single-walled carbon nanotube bundles by dielectrophoresis and Raman spectroscopy. *Appl. Phys. Lett.* **2008**, *92*.
- (22) (a) Wang, H.; Zhou, W.; Ho, D. L.; Winey, K. I.; Fischer, J. E.; Glinka, C. J.; Hobbie, E. K. Dispersing single-walled carbon nanotubes with surfactants: A small angle neutron scattering study. *Nano Lett.* **2004**, *4*, 1789–1793. (b) Yurekli, K.; Mitchell, C. A.; Krishnamoorti, R. Small-angle neutron scattering from surfactant-assisted aqueous dispersions of carbon nanotubes. *J. Am. Chem. Soc.* **2004**, *126*, 9902–9903.
- (23) (a) Inam, F.; Heaton, A.; Brown, P.; Peijs, T.; Reece, M. J. Effects of dispersion surfactants on the properties of ceramic-carbon nanotube (CNT) nanocomposites. *Ceram. Int.* **2014**, *40*, 511–516. (b) Vaisman, L.; Marom, G.; Wagner, H. D. Dispersions of surface-modified carbon nanotubes in water-soluble and water-insoluble polymers. *Adv. Funct. Mater.* **2006**, *16*, 357–363.
- (24) (a) Badaire, S.; Poulin, P.; Maugey, M.; Zakri, C. In situ measurements of nanotube dimensions in suspensions by depolarized dynamic light scattering. *Langmuir* **2004**, *20*, 10367–10370. (b) Lucas, A.; Zakri, C.; Maugey, M.; Pasquali, M.; van der Schoot, P.; Poulin, P. Kinetics of Nanotube and Microfiber Scission under Sonication. *J. Phys. Chem. C* **2009**, *113*, 20599–20605. (c) Shetty, A. M.; Wilkins, G. M. H.; Nanda, J.; Solomon, M. J. Multiangle Depolarized Dynamic Light Scattering of Short Functionalized Single-Walled Carbon Nanotubes. *J. Phys. Chem. C* **2009**, *113*, 7129–7133.
- (25) Strano, M. S.; Moore, V. C.; Miller, M. K.; Allen, M. J.; Haroz, E. H.; Kittrell, C.; Hauge, R. H.; Smalley, R. E. The role of surfactant adsorption during ultrasonication in the dispersion of single-walled carbon nanotubes. *J. Nanosci. Nanotechnol.* **2003**, *3*, 81–86.
- (26) Matarredona, O.; Rhoads, H.; Li, Z. R.; Harwell, J. H.; Balzano, L.; Resasco, D. E. Dispersion of single-walled carbon nanotubes in aqueous solutions of the anionic surfactant NaDDBS. *J. Phys. Chem. B* **2003**, *107*, 13357–13367.

(27) Lu, K. L.; Lago, R. M.; Chen, Y. K.; Green, M. L. H.; Harris, P. J. F.; Tsang, S. C. Mechanical damage of carbon nanotubes by ultrasound. *Carbon* **1996**, *34*, 814–816.

(28) Mukhopadhyay, K.; Dwivedi, C. D.; Mathur, G. N. Conversion of carbon nanotubes to carbon nanofibers by sonication. *Carbon* **2002**, *40*, 1373–1376.

(29) (a) Huang, Y. Y.; Knowles, T. P. J.; Terentjev, E. M. Strength of Nanotubes, Filaments, and Nanowires From Sonication-Induced Scission. *Adv. Mater.* **2009**, *21*, 3945. (b) Pagani, G.; Green, M. J.; Poulin, P.; Pasquali, M. Competing mechanisms and scaling laws for carbon nanotube scission by ultrasonication. *Proc. Natl. Acad. Sci. U.S.A.* **2012**, *109*, 11599–11604.

(30) Sesis, A.; Hodnett, M.; Memoli, G.; Wain, A. J.; Jurewicz, I.; Dalton, A. B.; Carey, J. D.; Hinds, G. Influence of Acoustic Cavitation on the Controlled Ultrasonic Dispersion of Carbon Nanotubes. *J. Phys. Chem. B* **2013**, *117*, 15141–15150.

(31) Sobolkina, A.; Mechtcherine, V.; Khavrus, V.; Maier, D.; Mende, M.; Ritschel, M.; Leonhardt, A. Dispersion of carbon nanotubes and its influence on the mechanical properties of the cement matrix. *Cem. Concr. Compos.* **2012**, *34*, 1104–1113.

(32) ISO 13320:2009. Particle size analysis – Laser diffraction methods, 2009.

(33) Ju, L.; Zhang, W.; Wang, X. J.; Hu, J. D.; Zhang, Y. L. Aggregation kinetics of SDBS-dispersed carbon nanotubes in different aqueous suspensions. *Colloids Surf., A* **2012**, *409*, 159–166.